Babaye Abdollahi et al., *BioImpacts,* 2022, 12(x), x-x
doi: 10.34172/bi.2022.23682
http://bi.tbzmed.ac.ir/

Synthesis and characterization of actively HER-2 Targeted Fe_3O_4@Au nanoparticles for molecular radiosensitization of breast cancer

Behnaz Babaye Abdollahi[1,2], Marjan Ghorbani[3], Hamed Hamishehkar[1], Reza Malekzadeh[2], Ali Reza Farajollahi[1,2,4*]

[1]Drug Applied Research Center, Tabriz University of Medical Sciences, Tabriz, Iran
[2]Department of Medical Physics, School of Medicine, Tabriz University of Medical Sciences, Tabriz, Iran
[3]Nutration Research Center, Tabriz University of Medical Sciences, Tabriz, Iran
[4]Imam Reza Educational Hospital, Radiotherapy Department, Tabriz University of Medical Sciences, Tabriz, Iran

Article Info

Article Type:
Original Article

Article History:
Received: 14 Feb. 2021
Revised: 4 Dec. 2021
Accepted: 7 Dec. 2021
ePublished: 15 Jan. 2022

Keywords:
Breast cancer
Radiation therapy
Active targeting
Trastuzumab
Au nanoparticles

Abstract

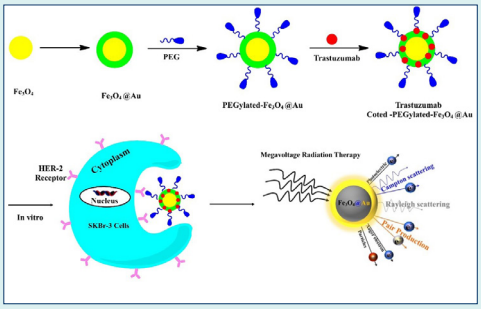

Introduction: The present study was done to assess the effect of molecularly-targeted core/shell of iron oxide/gold nanoparticles (Fe_3O_4@AuNPs) on tumor radiosensitization of SKBr-3 breast cancer cells.

Methods: Human epidermal growth factor receptor-2 (HER-2)-targeted Fe_3O_4@AuNPs were synthesized by conjugating trastuzumab (TZ, Herceptin) to PEGylated (PEG)-Fe_3O_4@AuNPs (41.5 nm). First, the Fe_3O_4@Au core-shell NPs were decorated with PEG-SH to synthesize PEG-Fe_3O_4@AuNPs. Then, the TZ was reacted to OPSS-PEG-SVA to conjugate with the PEG-Fe_3O_4@AuNPs. As a result, structure, size and morphology of the developed NPs were assessed using Fourier-transform infrared (FT-IR) spectroscopy, dynamic light scattering (DLS) and transmission electron microscopy (TEM), and ultraviolet-visible spectroscopy. The SKBr-3 cells were treated with different concentrations of TZ, Fe_3O_4@Au, and TZ-PEG-Fe_3O_4@AuNPs for irradiation at doses of 2, 4, and 8 Gy (from X-ray energy of 6 and 18 MV). Cytotoxicity was assessed by MTT assay, BrdU assay, and flow cytometry.

Results: Results showed that the targeted TZ-PEG-Fe_3O_4@AuNPs significantly improved cell uptake. The cytotoxic effects of all the studied groups were increased in a higher concentration, radiation dose and energy-dependent manner. A combination of TZ, Fe_3O_4@Au, and TZ-PEG-Fe_3O_4@AuNPs with radiation reduced cell viability by 1.35 ($P=0.021$), 1.95 ($P=0.024$), and 1.15 ($P=0.013$) in comparison with 8 Gy dose of 18 MV radiation alone, respectively. These amounts were obtained as 1.27, 1.58, and 1.10 for 8 Gy dose of 6 MV irradiation, respectively.

Conclusion: Radiosensitization of breast cancer to mega-voltage radiation therapy with TZ-PEG-Fe_3O_4@AuNPs was successfully obtained through an optimized therapeutic approach for molecular targeting of HER-2.

Introduction

Breast cancer is the second cancer-related cause of death in women and the most common type of cancer among women after skin cancers.[1] Currently, over 80% of patients with breast cancer undergo radiotherapy (RT) in their course of treatment. In RT, it is important to provide a high dose of radiation to tumor to kill cancerous cells while saving nearby surrounding healthy tissues.[2]

Adams et al, for the first time in 1977 reported chromosomal damage in the patient who had coronary angiography with iodine dye.[3] It has been found that the contrast media with high atomic number enhanced radiation damage at the loaded cells due to photoelectric effect.[4] Shortly after advent of nanotechnology, diagnostic and therapeutic values of nanoparticles (NPs) with high atomic number were quickly identified and studies introducing NPs into cancerous cells led to promising therapeutic effect by enhancing local energy transfer to tumor. Introducing NPs into cancerous cells enhances local energy transferred to tumor and accordingly, increases radiation-induced tumor damage while decreasing unwanted damage to surrounding healthy tissue.[5]

It is currently well-known that the mechanisms by which radiation induces damage to NPs-loaded cells have

*Corresponding author: Ali Reza Farajollahi, Email: afarajollahi@hotmail.com

three physical, chemical, and biological components. Even with only a small amount of NPs with high atomic number (Z) in tumor cells, the photoelectric effect (for kVp range, the photoelectric effect interaction probability varies with Z^4) and pair production (for photon energies >1.022 MeV) cross-section are significantly increased and considerably more energy per unit of mass is adsorbed than surrounding healthy tissue. Because, atomic cross-section for pair production shows a Z^2 dependence, the potentially absorbed energy for gold NPs (AuNPs, atomic number =79) is approximately 127 times ($79^2/7^2$) more than that of soft tissue.[6] Moreover, due to their higher density, Compton scattering probability is increased in comparison with soft tissue depending on incident energy.

The chemical phase involves formation of oxidative stress in tissues. In this phase, the main mechanism of cellular toxicity of NPs (about 60%) is through production of reactive oxygen species (ROS), leading to subsequent formation of oxidative stress. This results in DNA damage, unregulated cell signaling, cell toxicity, apoptosis, and cell cycle arrest. Geng et al found that AuNPs promoted intracellular ROS production in SKOV-3 human ovarian cancer cells when exposed to 90 kVp or 6 megavoltage (MV) X-rays.[7]

Recently core-shell NPs have been introduced to enhance performance of single-material NPs. The core-shell NPs have unique capabilities compared to single NPs, such as (i) less cytotoxicity (ii) bio- and cyto-compatibility, and (iii) better binding to other biologically active molecules.[8] It is crucial to enhance specificity of the drugs-loaded NPs in order to send more therapeutic agents to the targeted cells by specific ligands of corresponding receptors, overexpressed on cancer cells' membrane.[9] Cancer progression is often associated with overexpression of specific proteins called as tumor antigens, which can be used as biological markers to distinguish cancer cells from healthy counterparts.[10,11] Human epidermal growth factor receptor-2 (HER-2) has often been described as a marker for the targeted drug delivery to HER-2 -expressing cancer cells. HER-2 is overexpressed in about 20%–30% of breast cancer cases.[12] In chemotherapy, HER-2 is the main target for monoclonal antibody trastuzumab (TZ, Herceptin), which is very effective for patients with metastatic breast cancer. TZ not only targets breast cancer cells and accumulates in tumor, but also stops cell proliferation.[13] Au-coated NPs are significantly biocompatible and react easily with biomolecules, enabling the targeted delivery due to binding of proteins or antibodies. That is why core-shell NPs with Au shell have many biological applications.

Numerous studies have reported the positive effect of AuNPs on increasing radiation sensitivity, and on the other hand, applications of Fe_3O_4 NPs in magnetic resonance imaging (MRI) and hyperthermia have been well documented today. According to results of our previous studies on single Au and Fe_3O_4 NPs in RT and MRI,[14] in this study, we seek to combine these two serviceable NPs as a multifunctional nano-complex with simultaneous use in cancer diagnosis and treatment. Therefore, it is attempted to investigate therapeutic efficiency of the TZ-PEG-Fe_3O_4@AuNPs on SKBr-3 breast cancer cells in the presence of 6 and 18 MV radiation doses of photon RT. It is eventually expected that improving surface properties of Fe_3O_4@AuNPs for the targeted delivery can considerably increase cellular uptake and cytotoxicity. Due to high volume of data and experiments, in this paper, only the results related to RT section are mentioned.

Materials and Methods

Materials

Ferric chloride hexahydrate ($FeCl_3$-$6H_2O$), ferrous chloride tetrahydrate ($FeCl_2$, $4H_2O$), ammonia solution (25%), perchloric acid ($HClO_4$, 70–72 %), 1,4-dioxane, dimethyl sulfoxide (DMSO), sodium citrate dehydrate, ammonia solution (25–28%), and Hydrogen tetrachloroaurate (III) trihydrate ($HAuCl_4$) were purchased from Merck Chemicals. Orthopyridyldisulfide-polyethyleneglycol-N-hydroxysuccinimide (OPSS-PEG-SVA, molecular weight 5 kDa) was obtained from Laysan Bio and used as received. Thiolated polyethylene glycol (PEG-SH, molecular weight 2 kDa) was obtained from Iris Biotech GmbH, Marktredwitz, Germany and used as received. The breast carcinoma cell (SKBr-3) was purchased from the National Cell Bank of Iran, Pasteur Institute. Distilled water was used throughout the experiments. A vial containing 150 mg of TZ (Herceptin, Roche, Basel, Switzerland) was obtained from the "Oncology Research Center, Tabriz University of Medical Sciences".

Synthesis of Fe_3O_4 NPs

Iron oxide (Fe_3O_4) NPs were synthesized according to the method presented in the literature.[15] Briefly, 4 mL of ferric chloride solution (1 M) and 1 mL of ferrous chloride solution (2 M, in 2N hydrochloride) were mixed and added to 50 mL of ammonia solution (0.7 M). After stirring the solution for 30 minutes, the precipitate was obtained by magnetic separation and was mixed with 50 mL of diluted $HClO_4$ (2 M). Finally, the colloidal suspension was separated by centrifugation and the rest of it was diluted with water to reach 50 mL of concentration.

Preparation of Fe_3O_4@AuNPs

For synthesis of the Fe_3O_4@AuNPs, $HAuCl_4$ aqueous solution (5 mL, 3 mg/mL) was added to 40 mL of deionized (DI) water and was heated until boiling. Then, 2 mL of as-prepared Fe_3O_4 NPs and sodium citrate (2 mL, 40 mM) was added to the mixture and was stirred vigorously until the solution color changed from brown to burgundy. The solution color slowly changed from brown to burgundy under intense stirring.[16]

Conjugation of TZ to OPSS-PEG-SVA

TZ was initially PEGylated by reacting with a bifunctional

cross linker [orthopyridyldisulfide-polyethyleneglycol-N-hydroxysuccinimide (OPSS-PEG-SVA, Laysan Bio, Arab, AL), molecular weight 5 kDa]. Briefly, 500 μL of TZ (1 µg/µL, PBS, pH 6.0) was reacted with the OPSS-PEG-SVA (250 µL, 100 mM $NaHCO_3$) overnight at 4°C. The conjugates were then purified and buffer exchanged into PBS, pH 7.5, using ultrafiltration [Vivaspin 30 kDa MW cutoff].[17]

Preparation of TZ-Conjugated PEGylated Fe_3O_4@AuNPs (TZ-PEG-Fe_3O_4@AuNPs)

The thiol-terminus of the PEG linker was used to covalently bind the immunoconjugates to Fe_3O_4@AuNPs using the well-recognized strong gold-thiol interaction. Briefly, TZ-PEG-Fe_3O_4@AuNPs were prepared by first adding 40 µL of 250 µM PEG-SH to the Fe_3O_4@AuNPs (1 mL, 1mg/mL) and then immediately adding 200 µg TZ-PEG-OPSS in PBS, pH 7.5 and then allowed to proceed for 1 hour at 4°C.[18] The TZ-PEG-Fe_3O_4@AuNPs were purified by a permanent magnet at 4°C for 24 hours. One milliliter of the supernatant was removed, and the pellet was resuspended by adding 1 mL of PBS, pH 7.5. In order to determine the loading efficiency of TZ-PEG-OPSS conjugation, the unloaded TZ-PEG-OPSS was separated from the TZ-PEG-Fe_3O_4@AuNPs by means of an external magnet and then its concentration determined by the standard protocol of Bradford assay for quantifying the concentration of the protein in the supernatant.[19] The conjugation percentage of TZ-PEG-OPSS on the surface of Fe_3O_4@AuNPs was found to be 73 %.[20] Schematic of synthesis steps of new smart NPs with surface modification by TZ is presented in Fig. 1.

Characterization of NPs

FT-IR spectrometry

Chemical structures of the synthesized TZ-PEG-Fe_3O_4@AuNPs, and Fe_3O_4@AuNPs were specified by a Fourier-transform infrared (FT-IR) spectroscopy device (JASCO, Tokyo, Japan).

DLS and zeta potential measurement

Hydrodynamic diameters and zeta potential of TZ-PEG-Fe_3O_4@AuNPs and Fe_3O_4@AuNPs were assessed by dynamic light scattering (DLS) using a Nano Zeta-Sizer (DTS1060, Malvern Instruments, Malvern, UK).

Transmission electron microscopy

Internal structure, shape, and size of Fe_3O_4@AuNPs were assessed using transmission electron microscopy (TEM; JEM-1400, JEOL, Peabody, MA, USA). Size distribution of Fe_3O_4@AuNPs was calculated by ImageJ software (NIH, Bethesda, MD).

UV-Vis absorption spectra

The ultraviolet-visible (UV-Vis) spectroscopy was used to confirm correct synthesis of Fe_3O_4@AuNPs and to ensure loading of PEG and TZ antibodies on Fe_3O_4@AuNPs using a JASCO spectrophotometer (Model V-570, JASCO Inc., Japan).

X-ray diffraction (XRD) analysis

X-ray diffraction patterns of the synthesized Fe_3O_4@AuNPs, PEG-Fe_3O_4@AuNPs, and TZ-PEG-Fe_3O_4@AuNPs were obtained using an X-ray diffractometer (D5000,

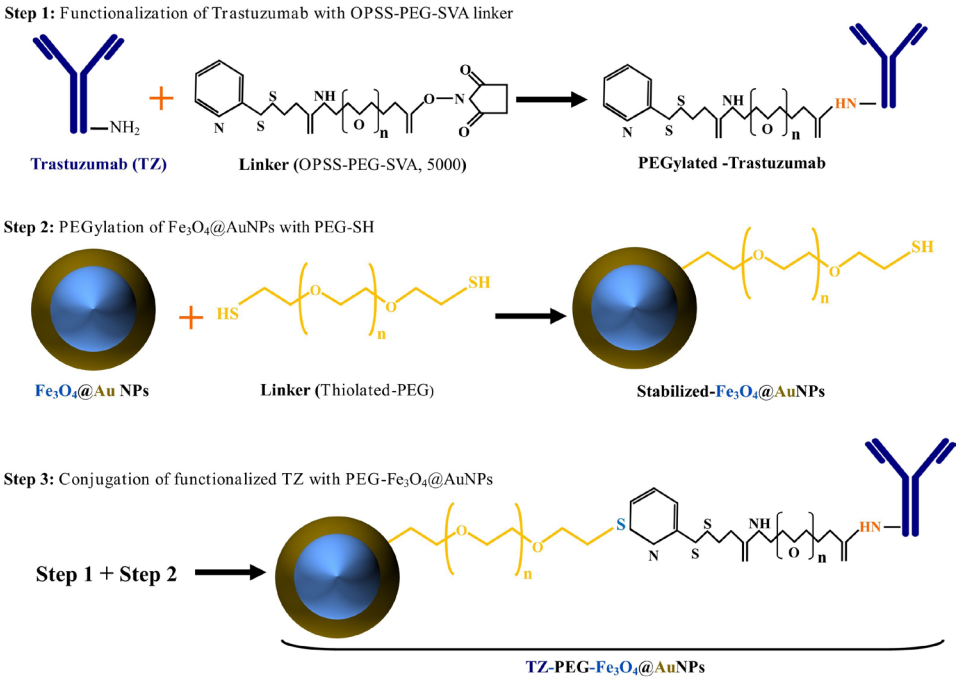

Fig. 1. Schematic illustration of the synthesis of trastuzumab (TZ)-loaded poly ethylene glycol (PEG)-Fe_3O_4@Au nanoparticles (NPs) (TZ-PEG-Fe_3O_4@AuNPs). Step 1: functionalization of TZ with orthopyridyldisulfide-polyethyleneglycol-N-hydroxysuccinimide (OPSS-PEG-SVA) linker, Step 2: PEGylation of Fe_3O_4@AuNPs by PEG-SH (PEG-Fe_3O_4@AuNPs), Step 3: conjugation of functionalized TZ with PEG-Fe_3O_4@AuNPs.

Siemens, Germany) with Cu Kα radiation at 40 kV in the range of 2θ from 20° to 80°.

Vibrating-sample magnetometer analysis

Vibrating-sample magnetometer (VSM; AGFM, Iran) was used to study the magnetic properties of the synthesized Fe_3O_4NPs, PEG-Fe_3O_4@AuNPs, and TZ-PEG-Fe_3O_4@AuNPs NPs at room temperature.

Cellular uptake

Qualitative evaluation of cellular uptake and subcellular distribution of Fe_3O_4@AuNPs, TZ-PEG-Fe_3O_4@AuNPs and was performed by fluorescence microscopy and flow cytometry assays. Rhodamine-labelled TZ-PEG-Fe_3O_4@AuNPs and Fe_3O_4@AuNPs were prepared as follows: rhodamine (5 mg) was dissolved in DMSO (1 mL) and then 50 µL of the solution was added to the TZ-PEG-Fe_3O_4@AuNPs and Fe_3O_4@AuNP suspensions (1 mL, 1 mg/mL). Afterward, sodium carbonate buffer (500 µL, 1 M) was added to the suspension and stirred for 20 hours. The excess rhodamine was removed by the Amicon® filter (molecular weight cutoff 100 kDa, Millipore, UK). Rhodamine-labelled TZ-PEG-Fe_3O_4@AuNPs and Fe_3O_4@AuNP were washed with double distilled water several times.[16] Cells were plated onto six-well plates at a density of 1.5×10^4 cells/plate. Cells with a density of 80% confluence were treated with rhodamine-labeled TZ-PEG-Fe_3O_4@AuNPs and rhodamine-labeled Fe_3O_4@AuNPs. After the cells were trypsinized and washed with PBS, cellular uptake was assessed by the flow cytometer (BD FACSCalibur, San Jose, CA, USA) based on fluorescence intensity. Cellular uptake of samples was studied after incubation with SKBr-3 cell lines for 1 and 4 hours.

MTT assay

The cell cytotoxicity of TZ, Fe_3O_4@AuNPs, and TZ-PEG-Fe_3O_4@AuNPs samples were assessed by MTT assay. The cells were seeded into 96-well plates (density of 1×10^4 cells/well) and incubated for 24 hours. Cytotoxicity of Fe_3O_4@AuNPs and TZ-PEG-Fe_3O_4@AuNPs were evaluated at different concentrations for 24 hours. MTT assay was performed based on the method that explained in our previous study: 200 µL of the MTT solution (5 mg/mL) was added (poured) to each well. Four hours later, 200 µL of DMSO was added to each well to dissolve the reactive dye. The optical density (OD) of each cell sample was read using an ELISA plate reader (Awareness Technology, Palm City, FL, USA) at 570 nm. The control well containing only medium, was used to set the absorption value to zero. All tests were performed three times and the averaged values were used to draw the cell viability curves.

Cell irradiation

Irradiation of SKBr-3 cells was performed using megavoltage X-ray beams at the Imam Reza Radiotherapy Department (The Imam Reza Educational Hospital, Tabriz City, East Azerbaijan Province, Iran). The samples were irradiated to the absorbed doses of 0, 2, 4, and 8 Gy from radiation beams of 6 MV (with dose rate of 300 MU/min) and 18 MV (with dose rate of 500 MU/min) using Siemens ONCOR Linear Accelerator (Siemens AG, Henkestr, Erlangen, Germany).

For uniform radiation to all cells, cell-plates should be filled with water and placed around the treated cell-plate to provide a full scatter environment with 16*12 cm^2 of field size and 100 cm of source -axis -distance (SAD) (Fig. 2). In addition, the cell plates were placed on top of 5-cm slab of polystyrene at center of the beam with adequate build-up to provide sufficient backscatter. The irradiated and control cells were returned to the incubator immediately after irradiation.

BrdU assay

The inhibitory effect of radiation, TZ, Fe_3O_4@AuNPs, and TZ-PEG-Fe_3O_4@AuNPs on proliferation of SKBr-3 cells was also measured by level of Bromo-deoxy-uridine (BrdU) incorporated into DNA of SKBr-3 cells using BrdU kit (BrdU Cell Proliferation ELISA Kit, colorimetric, Abcam, Cambridge, MA, USA). In short, cells were cultured within 96-well plates and were treated with TZ, Fe_3O_4@AuNPs, and TZ-PEG-Fe_3O_4@AuNPs (400 µg/mL). After 24 hours, the treated cells were exposed to 8 Gy of 6 and 18 MV radiation doses and were incubated for the next 24 hours. Then, BrdU solution (90 µL) was added to the cells and using FixDenat solution, the cells were fixed and their DNA was denatured. Cells were incubated for 24 hours at room temperature. Finally, amount of absorbance was determined by an enzyme-linked immunosorbent assay (ELISA) reader.

Cell cycle analysis

The apoptosis of studied groups before and after irradiation was investigated by propidium iodide (PI, a DNA dye that emits fluorescence upon binding to the double stranded DNA of living cells) staining test and flow-cytometry device. The SKBr-3 cells were treated with TZ Fe_3O_4@AuNPs, and TZ-PEG-Fe_3O_4@AuNPs (400 mg/mL) for 24 hours. They analyzed by using PI before and after exposure to 6 and 18 MV radiation beam (absorbed dose of 8 Gy).

For the analysis, the cells (5×10^5 per well) that were

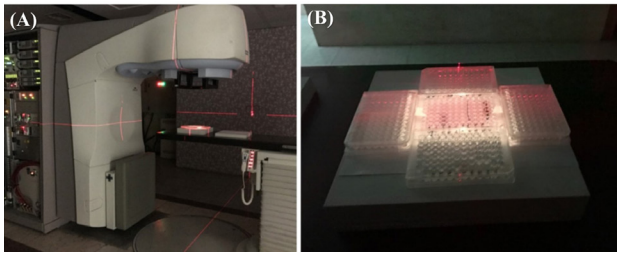

Fig. 2. Experimental set up. How to place cells for radiation in a radiotherapy device (A); How to place water-filled plates around the cells plate in the radiation field (B).

treated and irradiated after 24 hours, were washed twice using warm FBS, fixed with ice cold ethanol (70%) and stored at −20°C. The fixed cells then, incubated at 4°C for one day. After centrifugation (2000 rpm) and washing with PBS, to ensure that only DNA is stained, the samples incubated for 30 minutes by Ribonuclease. Finally, cells were stained using PI Solution in dark place to measure fluorescent intensity by the Flow cytometer.

Statistical analysis

The experiments were done as a minimum of three independent replicates and presented as the mean ± standard deviation (SD). Differences between groups were analyzed by Student's *t* test and Wilcoxon analysis with 95% confidence interval using SPSS 22.0 analysis software (SPSS, Inc., Armonk, NY, USA). $P < 0.05$ was considered to indicate a statistically significant difference (*$P < 0.05$; ** $P < 0.01$).

Results

Preparation of Fe_3O_4@AuNPs

Firstly, the Fe_3O_4@Au core-shell NPs were prepared by reduction of $HAuCl_4$ with sodium citrate in the presence of Fe_3O_4 NPs. Then, the Fe_3O_4@AuNPs were decorated with PEG-SH to synthesize PEG-Fe_3O_4@AuNPs. Besides, TZ was reacted to OPSS-PEG-SVA to conjugate with the PEG-Fe_3O_4@AuNPs in order to increase their stability and biocompatibility.

Characterization of TZ-PEG-Fe_3O_4@AuNPs

The UV-Vis extinction spectra of the pure Fe_3O_4@AuNPs, PEG-Fe_3O_4@AuNPs, and TZ-PEG-Fe_3O_4@AuNPs are presented in Fig. 3A. Characteristic surface plasmon resonance (SPR) bond of Fe_3O_4@AuNPs was observed close to 525 nm. Modification of the Fe_3O_4@AuNPs' surface did not cause a significant change in their morphology and optical properties. It has been found that peak of SPR depends on physical size and an increase in size can cause it to change.[21] Morphology and size of the synthesized NPs were also evaluated by TEM. The core/shell structure of Fe_3O_4@AuNPs is clearly shown in Fig. 3B. The average diameter was about 25–30 nm for the Fe_3O_4@AuNPs.

The magnetization curves of bared Fe_3O_4 NPs, PEG-Fe_3O_4@AuNPs and TZ-PEG-Fe_3O_4@AuNPs at room temperature are illustrated in Fig. 3C. The saturation magnetization (Ms) values of free Fe_3O_4 NPs, PEG-Fe_3O_4@AuNPs, and TZ-PEG-Fe_3O_4@AuNPs were 59.7, 42.2 and 33.4 emu g^{-1}, respectively. Compared with uncovered Fe_3O_4, the decrease in Ms value may be due to the presence of a non-magnetic layer containing Fe_3O_4.[22,23] In addition, no hysteresis loop was seen in the curve, which indicates the superparamagnetic properties of TZ-PEG-Fe_3O_4@AuNPs.

The FT-IR spectra of TZ, Fe_3O_4@AuNPs, and TZ-PEG-Fe_3O_4@AuNPs are presented in Fig. 3(D). The peaks at 2930 cm^{-1}, 1420.90 cm^{-1}, and 995 cm^{-1} were similar to those observed in HER-2 sample spectrum. In addition, the peaks appeared at 3430.9 cm^{-1} and 1630.21 cm^{-1} corresponded to bonded amide (–NH-) stretching vibrations, further approving successful conjugation of TZ antibody to surface.[24]

The XRD spectra of the Fe_3O_4@AuNPs, PEG-Fe_3O_4@AuNPs and TZ-PEG-Fe_3O_4@AuNPs were shown in Fig. 3E. The six diffraction peaks visible at 2θ = 30, 35.63, 43, 54, 57.1, and 62.8 which can be attributed to the (220),

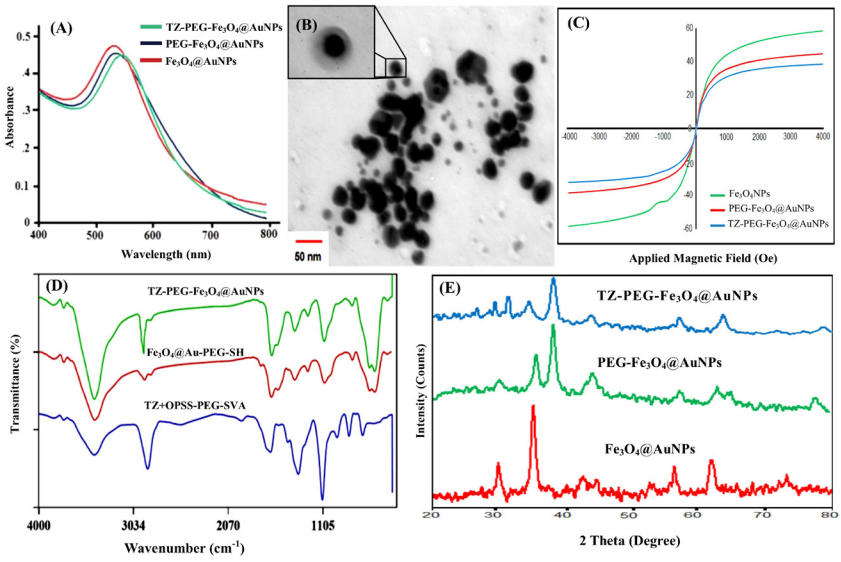

Fig. 3. Ultraviolet-visible (UV-vis) spectroscopy of the Fe_3O_4@AuNPs, PEG-Fe_3O_4@AuNPs and TZ-PEG-Fe_3O_4@AuNPs (A), Transmission electron microscope (TEM) images of the Fe_3O_4@Au core-shell NPs at different magnification (B), Magnetization versus applied magnetic field for the Fe_3O_4 NPs, PEG-Fe_3O_4@AuNPs and TZ-PEG-Fe_3O_4@AuNPs (C), Fourier transform infrared (FT-IR) spectra of TZ-PEG, PEG-Fe_3O_4@AuNPs and TZ-PEG-Fe_3O_4@AuNPs (D), XRD patterns of Fe_3O_4@AuNPs, PEG-Fe_3O_4@AuNPs and TZ-PEG-Fe_3O_4@AuNPs (E). Poly ethylene glycol (PEG).

(311), (400), (422), (511), and (440) plans of Fe_3O_4, respectively. Also, the peaks of Au - Fe_3O_4 describe both Au and Fe_3O_4 NPs, corresponding to Fe (220), (311), (511) and (440); and Au (111), (200), (220), (311), planes. Finally, the decresing of Fe_3O_4 peaks intensity depending on the Au shell thickness as well as the TZ-PEG coating polymer is shown.[18,23]

As seen in Table 1, the binding of PEG to Fe_3O_4@AuNPs increased the zeta potential from -23.2 mV to -3.4 mV. The increase of zeta potential to almost neutral charge for PEG-Fe_3O_4@AuNPs might be attributed to the presence of PEG chains which caused the complete shielding of the surface charges. Particle-size analysis showed that the Fe_3O_4@AuNPs had an average diameter of 30-40 nm (PDI = 0.195).

Table 1. The size, poly dispersity index (PDI) and zeta potential of developed naoparticles (NPs). Poly ethylene glycol (PEG) and trastuzumab (TZ)

Sample	Size by number (nm)	PDI	Zeta Potential (mV)
Fe_3O_4@AuNPs	32.6 nm	0.195	-23.2
PEG-Fe_3O_4@AuNPs	41.5 nm	0.219	-3.4
TZ-PEG-Fe_3O_4@AuNPs	67.4 nm	0.235	-41.5

Cellular uptake

As reported in previous literatures,[18] the cell uptake study of targeted NPs are investigated by two methods as follows: in one method, only the targeted NPs is evaluated on two cell lines with positive and negative receptors, and in the other method, both the targeted and non-targeted NPs are assessed on the cell line with only positive receptor. In both methods, the penetration of targeted NPs into cells with positive receptors is higher than that of (a) non-targeted NPs and (b) the cells without receptor. Because, the efficiency and accuracy are exactly the same in both methods, in the present work we used the second method to prove the higher penetration of NPs into cells with a positive receptor.

Intracellular uptake of NPs was confirmed by rhodamine-labelled Fe_3O_4@AuNPs and rhodamine-labelled TZ-PEG-Fe_3O_4@AuNPs by fluorescence microscopy (Fig. 4). Cells exposed to rhodamine-loaded TZ-PEG-Fe_3O_4@AuNPs showed better fluorescence activity than rhodamine-labelled untargeted Fe_3O_4@AuNPs.[18] Moreover, it was also observed that NPs' uptake was dependent on incubation time as reflected by the rise in fluorescence intensity (the maximum uptake was observed in case of rhodamine-loaded TZ-coated NPs in both periods). Therefore, higher cellular binding associated with NPs coated with TZ is probably due to their higher intracellular delivery by receptor- mediated endocytosis.[25]

In vitro cytotoxicity assay

Results regarding viability of SKBr-3 cells by different concentrations of TZ, Fe_3O_4@AuNPs, and TZ-PEG-

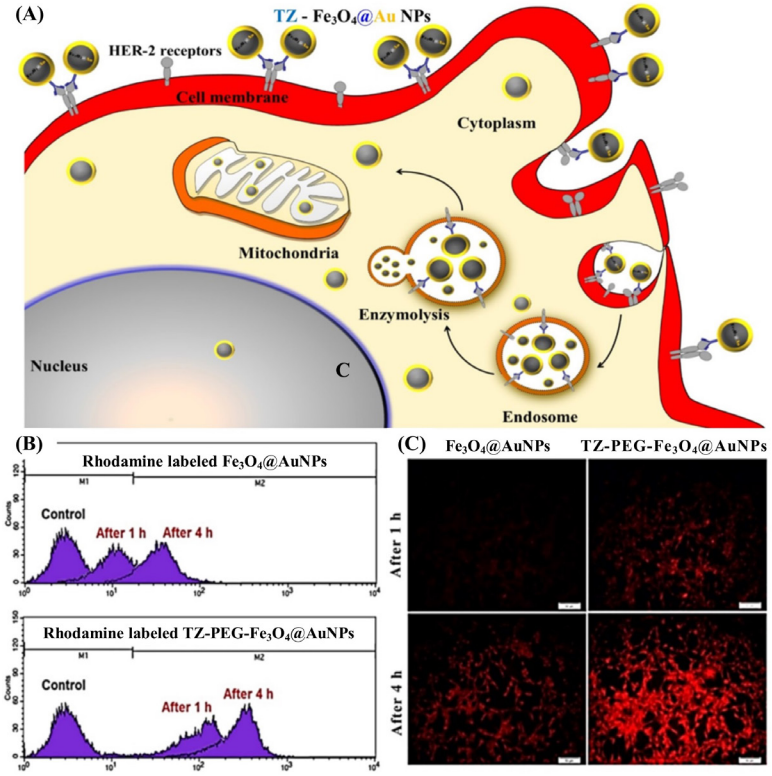

Fig. 4. Schematic illustration of the trastuzumab (TZ)-loaded poly ethylene glycol (PEG)-Fe_3O_4@Au nanoparticles (NPs) (TZ-PEG-Fe_3O_4@AuNPs) internalization (A), Cell uptake study of Fe_3O_4@AuNPs and TZ–PEG-Fe_3O_4@AuNPs after incubation with SKBr-3 cell lines after 1 h and 4 h (B); fluorescence microscopy images of treated SKBr-3 cell lines with Fe_3O_4@AuNPs and TZ-PEG-Fe_3O_4@AuNPs after 1 h and 4 h (C).

Fe_3O_4@AuNPs before and after exposure to 6 (2, 4, 8 Gy) and 18 MV (2, 4, 8 Gy) radiation doses are shown in Figs. 5A-C and 6AC), respectively. Fig. 5A clearly shows that at the same energy, the increase in radiation dose associated with more cellar damage and the greatest amount of cell damage occurred at 8 Gy. While, without using the NPs, cell viability was equal to 92% at 8 Gy and introduction of Fe_3O_4@AuNPs into the cell at concentrations of 31, 62, 125, 250, and 500 µg/mL reduced cell viability to 83.56%, 74.9%, 68.3%, 66.3%, and 53.3%, respectively. Fig. 5B depicts viability of the cells for 5, 10, 15, 20, 25, and 30 µg/mL of TZ concentration following radiation dose of 8 Gy. As can be seen from Fig. 5B, cell viability was obtained as 78.9%, 71.7%, 68.7%, 56.7%, 41.1%, and 33%, respectively. For treated cells with TZ-PEG-Fe_3O_4@AuNPs at radiation dose of 8 Gy, cell viability was equal to 77.6%, 69.8T, 64.7%, 53%, 33.2%, and 29.4%, respectively for the same concentrations (Fig. 5C).

According to the results presented in Fig. 6A, obviously, cellular damage is increased as radiation dose is increased, which was the case at both radiation energies. Cell viability was equal to 71%, 64.79%, 60.18%, 52.76%, and 43.69%, respectively for concentrations of 31, 62, 125, 250, and 500 µg/mL of Fe_3O_4@AuNPs in contrast to cell viability of 79% in the absence of NPs at the same radiation energy and absorbed dose. According to Fig. 6B, cell viability was observed as 66.36%, 60.59%, 53.59%, 47.40%, 33%, and 29.2%, respectively for 5, 10, 15, 20, 25, and 30 µg/mL of TZ concentration with radiation dose of 8 Gy. Fig. 6B also shows the effect of different concentrations of TZ on cell damage. As can be seen, increasing concentration of TZ from 5 to 30 µg/mL with 5 µg/mL increase interval in concentration, reduced cell viability from 66.36% to 29.2% at radiation dose of 8 Gy. For the treated cells with TZ-PEG-Fe_3O_4@AuNPs at radiation dose of 8 Gy, cell viability was obtained as 62.65%, 56.88%, 61.53%, 43.28%, 30.92%, and 27.62%, respectively for the same concentrations (Fig. 6C).

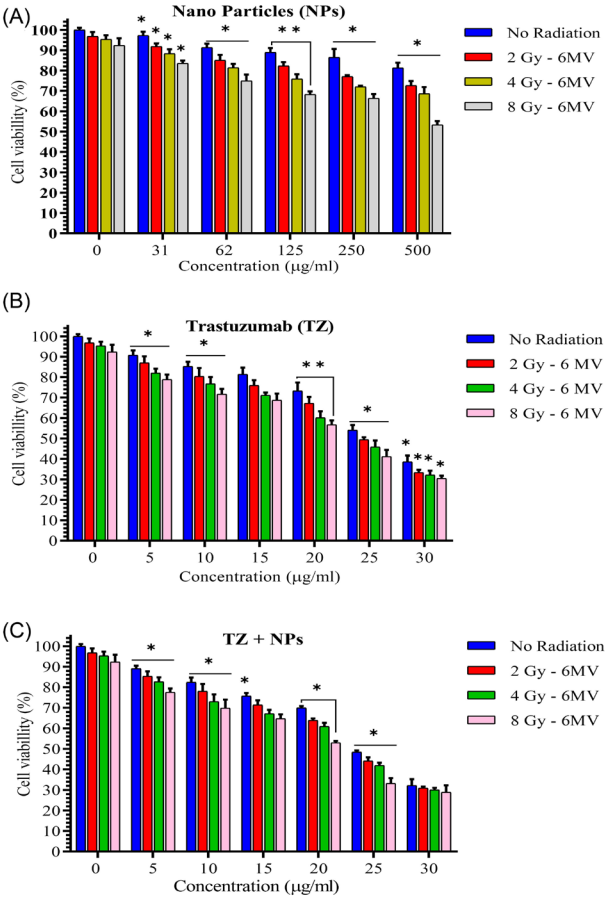

Fig. 5. Cell viability study by different concentrations of Fe_3O_4@Au nanoparticles (NPs) (A), Trastuzumab (TZ) (B) and TZ-PEG-Fe_3O_4@AuNPs (C) on SKBr-3 cell line after exposure to 6 MV (2, 4, 8 Gy) radiation. The x-axis represents the concentration (µg/mL) of NPs. Poly ethylene glycol (PEG). Each bar reveals the average value obtained from three samples. Asterisks indicate statistical significance (Student's *t* test; * $P<0.05$, ** $P<0.01$).

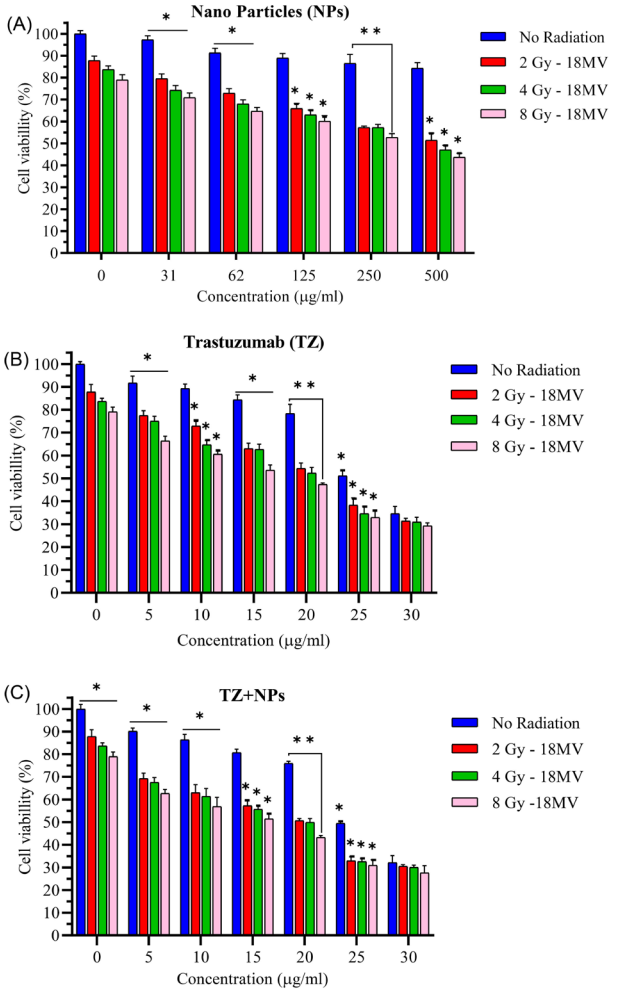

Fig. 6. Cell viability study by different concentrations of Fe_3O_4@Au nanoparticles (NPs) (A), Trastuzumab (TZ) (B) and TZ-PEG-Fe_3O_4@AuNPs (C) on SKBr-3 cell line after exposure to 18 MV (2, 4, 8 Gy) radiation. The x-axis represents the concentration (µg/mL) of NPs. Poly ethylene glycol (PEG). Each bar reveals the average value obtained from three samples. Asterisks indicate statistical significance (Student's t-test; * $P<0.05$, ** $P<0.01$).

Cell cycle analysis by flow cytometry

As shown in Fig. 7, cell population was higher in sub-G1 phase in the treated samples than the control sample, indicating a cell cycle arrest in sub- G1 phase. Results showed that early apoptotic rate in SKBr-3 cells treated with TZ, Fe_3O_4@AuNPs, and TZ-PEG-Fe_3O_4@AuNPs was equal to 7.24%, 8.67%, and 18.7%, respectively. While, with 18 MV of irradiation energy, cell viability of these groups was obtained as 9.42%, 37.2%, and 40.4%, respectively. According to the results, Fe_3O_4@AuNPs induced apoptosis in SKBr-3 cells in a radiation energy-dependent manner.

BrdU assay

The results of BrdU test for TZ, Fe_3O_4@AuNPs, and TZ-PEG-Fe_3O_4@AuNPs with and without radiation are shown in Fig. 8. As shown in Fig. 8, reduction by 83 and 72% was found in viability of the Fe_3O_4@Au-containing SKBr-3 cells when irradiated with radiation energies of 6 and 18 MV, respectively. Also, TZ antibodies reduced cell viability to 72% and 63%, and viability of the cells treated with TZ-PEG-Fe_3O_4@AuNPs was reduced by 56% and 41% in the presence of 6 and 18 MV radiation energies, respectively. The BrdU assay significantly displayed the decreased viability in SKBr-3 cells in the case of simultaneous use of 18 MV radiation beam and TZ-PEG-Fe_3O_4@AuNPs ($P<0.001$). These findings also revealed that cellular toxicity and apoptosis in SKBr-3 cells are strongly dependent on radiation energy ($P<0.02$).

Discussion

Along of their cytocompatibility and adaptable binding to biological molecules (antibodies), high atomic numbers nano-metals can be used in RT as sensitizers for therapeutic applications. A bimodal nano-agent was first prepared by synthesizing Fe_3O_4@AuNPs followed by labeling with TZ, for the therapeutics of HER-2 positive breast cancer cells.

The TEM image of Fe_3O_4@AuNPs, in which most of the

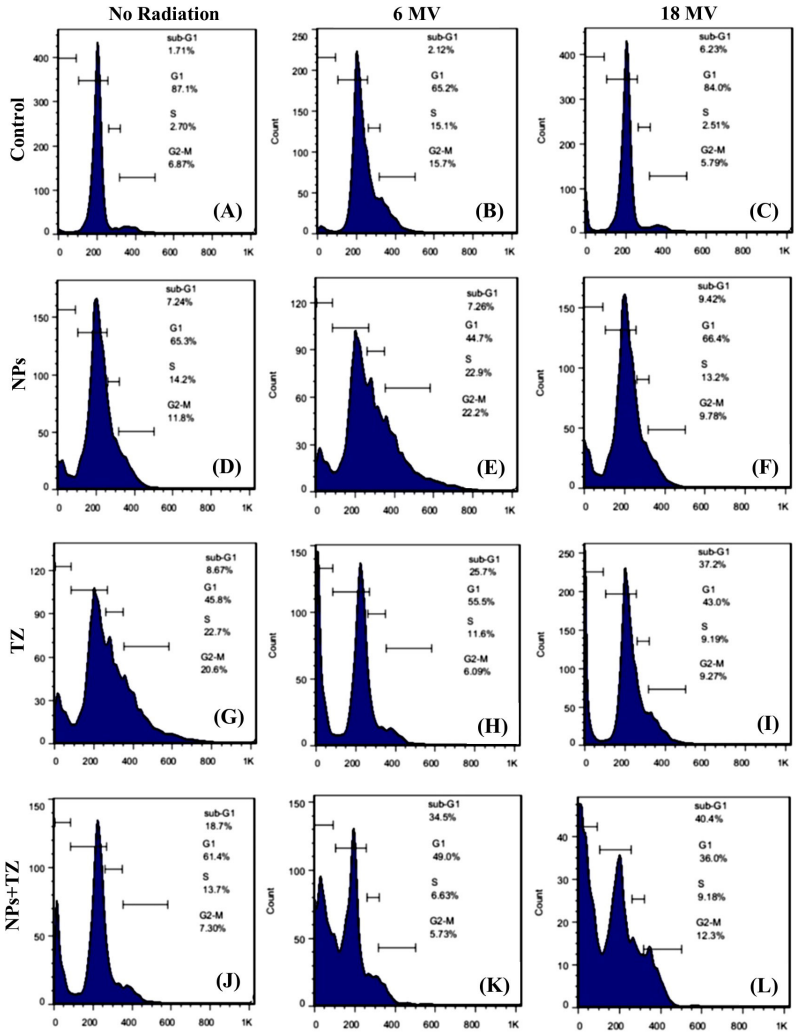

Fig. 7. Cell cycle distributions investigated for SKBr-3 cells. The untreated cells as control (A), cells treated with radiation 6 MV (8 Gy) (B), cells treated with radiation 18 MV (8 Gy) (C), cells treated with Fe_3O_4@Au nanoparticles (NPs) without radiation (D), cells treated with Fe_3O_4@AuNPs exposed to 6 MV radiation (E), and 18 MV radiation (F), cells treated with trastuzumab (TZ) without radiation (G), cells treated with TZ exposed to 6 MV radiation (H), and 18 MV radiation (I), cells treated with TZ-PEG-Fe_3O_4@AuNPs without radiation (J), cells treated with TZ-PEG-Fe_3O_4@AuNPs with 6 MV radiation (K), and 18 MV radiation (L). Poly ethylene glycol (PEG).

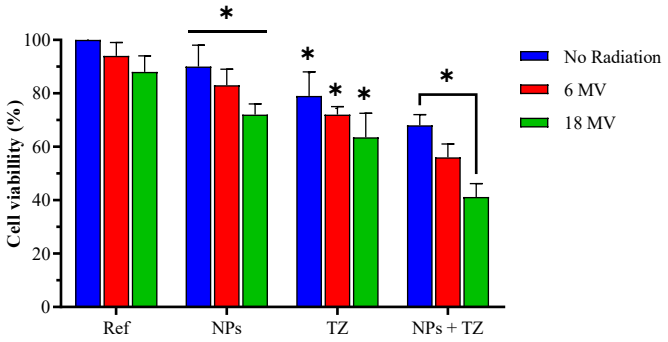

Fig. 8. Survival percentage of cells treated with Fe_3O_4@Au nanoparticles (NPs), Trastuzumab (TZ) and TZ-PEG-Fe_3O_4@AuNPs with and without of 8 Gy radiation at energies of 6 and 18 MV. Ref represents the cell survival of the untreated cells with NPs, TZ and NPs + TZ. Poly ethylene glycol (PEG). Each bar reveals the average value obtained from three samples. Asterisks indicate statistical significance (Student's *t* test; * P<0.05).

NPs are spherical in shape with an average diameter of 20-30 nm. The core-shell structure and uniform distribution of NPs are clearly shown. The FT-IR, XRD and UV-Vis results confirmed the presence of PEG on the surface of NPs, the effective coating of monoclonal antibody on the synthesized NPs. The XRD results illustrated in Fig. 3E are consistent with the crystal phases of Fe_3O_4 and standard XRD data for Fe_3O_4 (JCPDS card: 01-075-0033).[26] After PEG coating, the UV-Vis spectrum showed a slight red shift (527 nm). The antibody-conjugated NPs also showed a slight increase in the maximum absorption peak and a redshift of ~5 nm. Given to positive charge of antibody, the TZ-PEG-Fe_3O_4@AuNPs had higher zeta potential then untargeted NPs. This shift is consistent with the research conducted by Jian et al.[27] Also, the increase of zeta potential to almost neutral charge for PEG-Fe_3O_4@AuNPs might be attributed to the presence of PEG chains which caused the complete shielding of the surface charges.[28] Also, due to high swelling capacity of the NPs, it was observed that diameter of the particles measured by DLS was higher than that of the particles estimated by TEM. After conjugation of TZ to the NPs, there was a slight increase in particle size to 60-70 nm (PDI = 0.235).

As shown in Fig. 4, TZ-PEG-Fe_3O_4@AuNPs exhibited a higher cellular uptake than Fe_3O_4@AuNPs during 1 and 4 hours, respectively, which is due to HER-2 overexpression of breast cancer cells. Therefore, cell toxicity and drug concentrations within the cell were increased. These results are compared with those obtained from cell toxicity tests (MTT and cell cycle analysis), showing successful internalization of Fe_3O_4@AuNPs with TZ coating.

According to the Figs. 5 and 6, the TZ-PEG-Fe_3O_4@AuNPs showed higher inhibitory action in comparison with other samples. Enhanced inhibition of cell growth for TZ-PEG-Fe_3O_4@AuNPs would be advantageous in lowering radiation dose in RT. The results also showed that the surface-modified Fe_3O_4@AuNPs provide an efficient anti-cancer delivery system. Therefore, it can be claimed that dose can be reduced when using TZ-PEG-Fe_3O_4@AuNPs to have the same clinical response. It should be noted that the value of NPs is probably be very dominant in *in-vivo* by targeting tumor tissue because of their enhanced permeability and retention (EPR) effect, reduced drug side effects (an extremely important issue for cytotoxic anti-cancer agents), prolonged circulation time, and intact TZ biological activity. The successful performance of TZ-coated Fe_3O_4@AuNPs would be beneficial in lowering the administration dose of anticancer drugs thereby avoiding the associated dose-dependent side effects of TZ. Therefore, it can be concluded that the efficacy of nano-particulate systems in comparing to free drugs obtained when they test in the *in vivo* condition and it may be the reason that there is no significant difference in toxicity of cells between TZ-coated PEG-Fe_3O_4@AuNPs and free TZ in culture medium.

It should be mentioned that radiation at 6 MV (2, 4, and 8 Gy) did not cause significant toxicity on SKBr-3 cells (cell viability of 98%) and cell viability was obtained more than 79% at 18 MV (2, 4, and 8 Gy) (P>0.05). This may be due to radio-resistance of SKBr-3 cells. However, more cell death was observed at 18 MV compared to 6 MV at same dose of radiation (P<0.05). The effect of dose rate could be the possible explanation for these differences, 300 VS 500 MU/min. Several studies have investigated the effect of dose rates on different cell lines.[29,30] The inverse effect of dose rate has been also reported in some cells. For example, Mitchell et al, found that lowering dose rate from 1.54 to 0.37 Gy/h in HeLa cells resulted in more cell death.[31] Studies have shown significant changes in repair of sub-lethal damages for different cell. Darfarin et al investigated radiosensitization ability of Au@Si_2O core-shell NPs at 6 and 18 MV radiation energies at doses of 2, 4, and 8 Gy on MCF-7 cell line. They reported that at a constant absorbed dose, dose enhancement using 18 MV was more than 6 MV.[32]

According to these results, it can be concluded that, NPs with a radiation dose of 8 Gy at both 6 and 18 MV caused higher cytotoxicity in SKBr-3 cells compared to NPs and radiation groups alone at the same concentration and radiation dose (P<0.05). Our results showed that a combination of active targeted Fe_3O_4@AuNPs with radiation resulted in greater tumor cell death compared

to the untreated groups of NPs ($P < 0.01$). Clearly, tumor-targeted TZ-PEG-Fe_3O_4@AuNPs highly accumulating in tumor cells, indicate a remarkable advance in nano-medicine with widespread clinical applications. Here, TZ, as an admirable targeting antibody, helped to link to HER-2 receptor-expressing breast cancer cells.

The cytotoxic effects of all concentrations of the TZ and TZ-coated NPs were increased by increasing radiation dose and energy. These findings are in agreement with extensively reported studies.[33] Similarly, Cai et al assessed cytotoxicity of TZ-AuNP-^{111}In on SKBr-3 cell line in their *in vitro* study. TZ-AuNP-^{111}In was significantly bound to SKBr-3 cells and was more efficiently internalized than AuNP-^{111}In as a result, increased double-strand breaks in DNA. They found that cell viability in SKBr-3 cells was decreased by 55% using TZ-AuNP-^{111}In.[34]

The results of this study indicated that the introduced NPs can change cell cycle pattern in SKBr-3 cell line. Thus, the increase in cell population in sub-G1 following treatment of cells indicated induction of apoptosis and confirming the anti-proliferative effect of NPs and TZ with irradiation. These results are in accordance with results of studies, in which the increased apoptosis rate was found when chemotherapy together with NPs was applied for treatment of breast cancer cells.[35,36]

Similar results have been also reported by Darfarin et al, who showed that the amine and thiol-activated NPs (AuN@SiO_2 and AuS@SiO_2) as radiation sensitizers increased number of cells in the (G0-G1) phase. In cases where DNA damage is severe, the damaged cell destroys itself through apoptosis pathway. Flow cytometric studies showed that cell cycle response depends on cell type, dose rate, and even some cell lines exhibit threshold dose below which they do not respond to radiation and also, there is a dose threshold in some cell lines.[37] Matsuya et al investigated changes in cell cycle of CHO-K1 cells under various radiation dose rates. They observed different results regarding cell cycle: 1) cellular accumulation at G2 phase when exposed to low dose rate (about 1 Gy/h); 2) delay in DNA synthesis and accumulation of cells at S/G2 phase when exposed to moderate dose rate (about 3 Gy/h), and 3) stopping cell cycle at all checkpoints (G1/S and G2 /M phases) and delaying DNA synthesis when exposed to higher doses (about 6 Gy/h).[38]

The results of BrdU test are completely consistent with the results obtained from MTT and cell cycle tests. Simultaneous use of NPs, TZ, and radiation therapy increased the cytotoxic effects on SKBr-3 cells. In addition, BrdU assay results, in line with cell cycle analysis, showed the highest potential for cytotoxicity at 18 MV radiation energy. Besides, it was confirmed that Fe_3O_4@AuNPs and TZ are toxic in the absence of radiation.

Hainfeld et al reported capacity of AuNPs (1.9 nm) to control growth of breast cancer tumors when used in combination with 250 kVp X-rays (30 Gy). One-year survival was obtained as 86% versus 20% with X-rays alone.[39] Similarly, Rahman et al investigated the effect of enhancing radiation dose of different concentrations of AuNPs (1.9 nm) on BAE cells. They revealed that dose enhancement factor (DEF) was significantly increased using high concentration of NPs. DEFs of 24.6 and 4 were noted while using 1mM and 0.25 mM at 80 kVp, respectively.[40] However, Jain et al evaluated the combined cytotoxicity of AuNPs (1.9 nm) with 160 kVp X-rays. They reported an average DEF of 1.4 in MDA-MB-231 breast cancer cells.[27] Also, Butterworth et al studied radiation enhancement of AuNPs in several cell lines with two different concentrations at radiation energy of 160 kVp. They reported variable DEFs for various cell lines using 0.05 and 0.5 mM of AuNPs. DEFs of 0.86 and 0.87 for L 132 cell line, 1.16 and 1.97 for AGO cell line, and 1.30 and 1.91 for T98G cell line were obtained.[41] These diverse results raise several fundamental questions, including whether it is necessary to achieve intracellular delivery of NPs for enhancement of radiation dose.

Besides, whether penetration rate of NPs into these cell lines is the same, or whether achieving intracellular delivery of NPs is necessary to obtain an increase in dose of radiation therapy. The NPs accumulate firstly in tumors due to their leaky vasculature as a result of the well-known EPR effect.[42] In one of the first studies to investigate the radiosensitization effect of the targeted NPs, Kong et al assessed the influence of the modified glucose-coated AuNPs (Glu-AuNPs) in the MCF-7 cells together with 200 kVp X-rays. Results showed that although, non-targeted AuNPs were mainly limited to cell membrane; Glu-AuNPs entered cells and were distributed in cytoplasm. Predictably, Glu-AuNPs caused more cell death than non-targeted AuNPs, indicating that internalization is essential to enhance radiation dose of NPs.[43] Recently, Abhari et al investigated application of bovine serum albumin (BSA)-modified Bi_2S_3@AuNPs bonded to folic acid (FA) as a targeted radiosensitizer for breast cancer therapy. They showed that FA could give a tumor-targeting ability, and BSA coating gives prolonged circulation time ability to NPs. The FA-functionalized Bi_2S_3@AuNPs demonstrated *in vitro* and *in vivo* enhanced tumor radiosensitization.[44]

Also, Chattopadhyay et al found that DNA damage in cells treated with TZ-PEG-AuNPs was 5 and 3.3 times higher than cells treated with PEG-AuNPs and control cells, respectively. Surface modification of AuNPs with TZ provided their binding to HER-2-exprssing cells, and then they entered cell cytoplasm through EPR process, causing high DNA damage due to biochemical and biophysical damage mechanisms.[45] A significant effect of radiation interaction and NPs inside cell was observed in case of increasing cell damage. As discussed previously, the Compton scattering and pair production at MV radiation range (above 5 MeV, pair production becomes dominant) produce scattered photons and secondary electrons, which mainly deposit their energy in-situ (Fig. 9).

Here, it was found that antibody was successfully

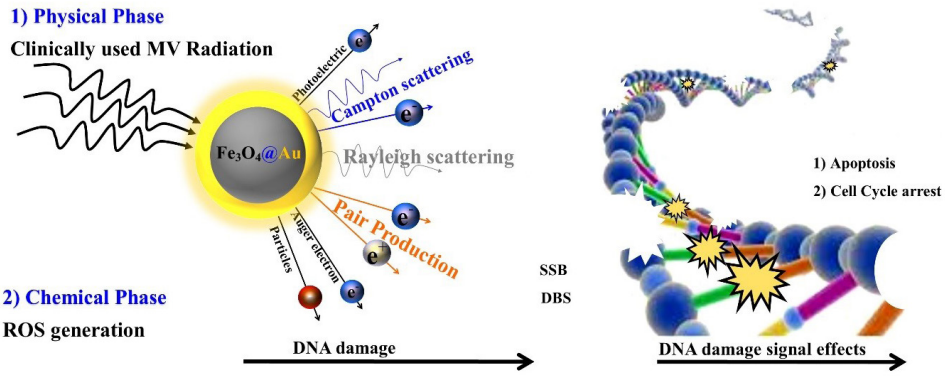

Fig. 9. Schematic presentation of the DNA damage during radio-sensitization by Fe_3O_4@Au nanoparticles (NPs). The two main mechanisms of cell death using radio-sensitizers are cell damage due to physical mechanism (pair production, Compton and photoelectric effects) and chemical mechanism (production of ROS and oxidative stress) lead to direct or indirect DNA damage and arrest the cell cycle or apoptosis.

conjugated to 30 nm Fe_3O_4@AuNPs, although it increased hydrodynamic size from 40 to 70 nm, it caused a significant binding with HER-2 receptors on cells. Evaluation of cell viability of SKBr-3 breast cancer cells, including the targeted and non-targeted Fe_3O_4@AuNPs exposed to 6 and 18 MV radiation energies indicated that internalization of Fe_3O_4@AuNPs by HER-2 receptor was necessary to decrease cell viability. The introduced molecularly targeted radiosensitizer in the current study could be used to treat other HER-2-receptor-expressing cancer cells. Despite all the efforts and innovations available, animal study of this proposal seems to be very interesting subject, which can be addressed by the authors in future studies.

Research Highlights

What is the current knowledge?

√ Megavoltage radiation therapy is one of the most common and effective cancer treatment modalities. Also, due to its side effects, numerous innovative methods have been proposed to enhance the effective dose of RT in cancer cells such as, using radio-sensitizers.

√ The core-shell NPs have unique capabilities compared to single NPs such as (i) less cytotoxicity (ii) bio- and cyto-compatibility, and (iii) better binding to other biologically active molecules for use as radio-sensitizers.

What is new here?

√ Fabrication of the stable and bio-compatible PEGylated Fe_3O_4@AuNPs targeted with trastuzumab (TZ) antibody as a new theranostic nano-agent (TZ-PEG-Fe_3O_4@AuNPs).

√ Radio-sensitization effects of the TZ-PEG-Fe_3O_4@AuNPs were investigated using 6 and 18 megavoltage RT for the first time.

√ Radiation of SKBr-3 cells in the presence of TZ-PEG-Fe_3O_4@AuNPs showed significant radio-sensitization.

√ The antibody conjugating to PEG-Fe_3O_4@AuNPs opens the way to produce radio-sensitizers with high-efficiency.

Conclusion

In this study, trastuzumab-loaded PEG-Fe_3O_4@Au core–shell NPs were successfully fabricated as radiation sensitizer. As shown in the results of MTT assay, BrdU assay, and cell cycle, the combination of targeted Fe_3O_4@AuNPs and radiation therapy showed a complementary effect in cells damage. As a result, the trastuzumab-loaded PEG-Fe_3O_4@AuNPs (as the targeted-NPs) along with radiation exhibited higher cytotoxicity against SKBr-3 than free trastuzumab and Fe_3O_4@AuNPs due to (a) the higher cellular uptake of SKBr-3 as a HER-2 positive breast cancer cell line and, (b) physical mechanism (Pair production, Compton and Photoelectric effects) and chemical mechanism (production of ROS and oxidative stress) of Fe_3O_4@AuNPs which lead to direct or indirect DNA damage of cells. The findings of this study could be useful for designing future cancer therapy strategies using bio-radio sensitizers combined with megavoltage range radiation therapy.

Acknowledgements

Authors like to acknowledge Tabriz University of Medical Sciences for the financial support current project.

Funding sources

This study was supported by the Drug Applied Research Center, Tabriz University of Medical Sciences, Tabriz, Iran.

Ethical statement

There is none to be disclosed.

Competing interests

None of the authors have any conflicting interests.

Authors' contribution

BBA: Preparation of nanoparticles, Data collection; MG: Experiments design, data analysis, provision of study materials and equipment; HH: Experiments design, provision of study materials and equipment, data analysis, writing and reviewing; RM: Original draft writing, Literature search, Data collection; AF: Study design, Data interpretation, supervision, writing and reviewing. All the authors read and approved the final manuscript.

References

1. Carol D, Rebecca S, Priti B, Ahmedin J. Breast cancer statistics, 2013. *CA Cancer J Clin* 2014; 64: 52-62. https://doi.org/10.3322/caac.21203
2. Hainfeld JF, Slatkin DN, Smilowitz HM. The use of gold nanoparticles to enhance radiotherapy in mice. *Phys Med Biol* 2004; 49: N309. https://doi.org/10.1088/0031-9155/49/18/n03
3. Adams FH, Norman A, Mello RS, Bass D. Effect of radiation and contrast media on chromosomes: preliminary report. *Radiology* 1977; 124: 823-6. https://doi.org/10.1148/124.3.823
4. Mello RS, Callisen H, Winter J, Kagan AR, Norman A. Radiation dose enhancement in tumors with iodine. *Med Phys* 1983; 10: 75-8. https://doi.org/10.1118/1.595378
5. Borran AA, Aghanejad A, Farajollahi A, Barar J, Omidi Y. Gold nanoparticles for radiosensitizing and imaging of cancer cells. *Radiat Phys Chem* 2018; 152: 137-44. https://doi.org/10.1016/j.radphyschem.2018.08.010
6. Retif P, Pinel S, Toussaint M, Frochot C, Chouikrat R, Bastogne T, et al. Nanoparticles for radiation therapy enhancement: the key parameters. *Theranostics* **2015**; 5: 1030. https://doi.org/10.7150/thno.11642
7. Geng F, Song K, Xing JZ, Yuan C, Yan S, Yang Q, et al. Thio-glucose bound gold nanoparticles enhance radio-cytotoxic targeting of ovarian cancer. *Nanotechnology* **2011**; 22: 285101. https://doi.org/10.5681/bi.2014.003
8. Chatterjee K, Sarkar S, Rao KJ, Paria S. Core/shell nanoparticles in biomedical applications. *Adv Colloid Interface Sci* **2014**; 209: 8-39. https://doi.org/10.1016/j.cis.2013.12.008
9. Shafaee A, Islamian JP, Zarei D, Mohammadi M, Nejati-Koshki K, Farajollahi A, et al. Induction of Apoptosis by a Combination of 2-Deoxyglucose and Metformin in Esophageal Squamous Cell Carcinoma by Targeting Cancer Cell Metabolism. *Iran J Med Sci* **2019**; 44: 99.
10. Amjadi S, Hamishehkar H, Ghorbani M. A novel smart PEGylated gelatin nanoparticle for co-delivery of doxorubicin and betanin: A strategy for enhancing the therapeutic efficacy of chemotherapy. *Mater Sci Eng C* **2019**; 97: 833-41. https://doi.org/10.1016/j.msec.2018.12.104
11. Ghorbani M, Hamishehkar H. Decoration of gold nanoparticles with thiolated pH-responsive polymeric (PEG-bp (2-dimethylamio ethyl methacrylate-co-itaconic acid) shell: A novel platform for targeting of anticancer agent. *Mater Sci Eng C* **2017**; 81: 561-70. https://doi.org/10.1016/j.msec.2017.08.021
12. Koo T, Kim IA. Brain metastasis in human epidermal growth factor receptor 2-positive breast cancer: from biology to treatment. *Radiat oncol J* **2016**; 34: 1. https://doi.org/10.3857/roj.2016.34.1.1
13. Bruno R, Washington CB, Lu J-F, Lieberman G, Banken L, Klein P. Population pharmacokinetics of trastuzumab in patients with HER2+ metastatic breast cancer. *Cancer Chemother Pharmacol* **2005**; 56: 361-9. https://doi.org/10.1007/s00280-005-1026-z
14. Mansouri H, Gholibegloo E, Mortezazadeh T, Yazdi MH, Ashouri F, Malekzadeh R, et al. A biocompatible theranostic nanoplatform based on magnetic gadolinium-chelated polycyclodextrin: in vitro and in vivo studies. *Carbohyd Polym* **2021**; 254: 117262. https://doi.org/10.1016/j.carbpol.2020.117262
15. Massart R. Preparation of aqueous magnetic liquids in alkaline and acidic media. *IEEE Trans Magn* **1981**; 17: 1247-8. https://doi.org/10.1109/TMAG.1981.1061188
16. Ghorbani M, Mahmoodzadeh F, Nezhad-Mokhtari P, Hamishehkar H. A novel polymeric micelle-decorated Fe_3O_4/Au core–shell nanoparticle for pH and reduction-responsive intracellular co-delivery of doxorubicin and 6-mercaptopurine. *New J Chem* **2018**; 42: 18038-49. https://doi.org/10.1039/C8NJ03310B
17. Dziawer Ł, Majkowska-Pilip A, Gaweł D, Godlewska M, Pruszyński M, Jastrzębski J, et al. Trastuzumab-modified gold nanoparticles labeled with 211At as a prospective tool for local treatment of HER2-positive breast cancer. *Nanomaterials* **2019**; 9: 632. https://doi.org/10.3390/nano9040632
18. Ghorbani M, Hamishehkar H, Arsalani N, Entezami AA. Preparation of thermo and pH-responsive polymer@ Au/Fe 3 O 4 core/shell nanoparticles as a carrier for delivery of anticancer agent. *J Nanopart Res* **2015**; 17: 1-13. https://doi.org/10.1007/s11051-015-3097-z
19. Niza E, Noblejas-López MdM, Bravo I, Nieto-Jiménez C, Castro-Osma JA, Canales-Vázquez J, et al. Trastuzumab-targeted biodegradable nanoparticles for enhanced delivery of Dasatinib in HER2+ Metastasic breast Cancer. *Nanomaterials* **2019**; 9: 1793. https://doi.org/10.3390/nano9121793
20. Lv S, Sheng J, Zhao S, Liu M, Chen L. The detection of brucellosis antibody in whole serum based on the low-fouling electrochemical immunosensor fabricated with magnetic Fe3O4@ Au@ PEG@ HA nanoparticles. *Biosens Bioelectron* **2018**; 117: 138-44. https://doi.org/10.1016/j.bios.2018.06.010
21. Liang R-P, Yao G-H, Fan L-X, Qiu J-D. Magnetic Fe3O4@ Au composite-enhanced surface plasmon resonance for ultrasensitive detection of magnetic nanoparticle-enriched α-fetoprotein. *Anal Chim Acta* **2012**; 737: 22-8. https://doi.org/10.1016/j.aca.2012.05.043
22. Liu S, Yu B, Wang S, Shen Y, Cong H. Preparation, surface functionalization and application of Fe3O4 magnetic nanoparticles. *Adv Colloid Interface Sci* **2020**; 281: 102165. https://doi.org/10.1016/j.cis.2020.102165
23. Zhao X, Cai Y, Wang T, Shi Y, Jiang G. Preparation of alkanethiolate-functionalized core/shell Fe3O4@ Au nanoparticles and its interaction with several typical target molecules. *Anal Chem* **2008**; 80: 9091-6. https://doi.org/10.1021/ac801581m
24. Cui Y-R, Hong C, Zhou Y-L, Li Y, Gao X-M, Zhang X-X. Synthesis of orientedly bioconjugated core/shell Fe3O4@ Au magnetic nanoparticles for cell separation. *Talanta* **2011**; 85: 1246-52. https://doi.org/10.1016/j.talanta.2011.05.010
25. Domínguez-Ríos R, Sánchez-Ramírez DR, Ruiz-Saray K, Oceguera-Basurto PE, Almada M, Juárez J, et al. Cisplatin-loaded PLGA nanoparticles for HER2 targeted ovarian cancer therapy. *Colloids Surf B* **2019**; 178: 199-207. https://doi.org/10.1016/j.colsurfb.2019.03.011
26. Revathy R, Kalarikkal N, Varma MR, Surendran KP. Exotic magnetic properties and enhanced magnetoelectric coupling in Fe3O4-BaTiO3 heterostructures. *J Alloys Compd* **2021**; 161667. https://doi.org/10.1016/j.jallcom.2021.161667
27. Jain J, Coulter A. Hounsell, KT Butterworth, SJ McMahon, WB Hyland, MF Muir, GR Dickson, KM Prise, FJ Currell, J. M. O'Sullivan, and DG Hirst,"Cell-specific radiosensitization by gold nanoparticles at megavoltage radiation energies,". *Int J Radiat Oncol Biol Phys* **2011**; 79: 531-9. https://doi.org/10.1016/j.ijrobp.2010.08.044
28. Ishii T, Otsuka H, Kataoka K, Nagasaki Y. Preparation of functionally PEGylated gold nanoparticles with narrow distribution through autoreduction of auric cation by α-biotinyl-PEG-block-[poly (2-(N, N-dimethylamino) ethyl methacrylate)]. *Langmuir* **2004**; 20: 561-4. https://doi.org/10.1021/la035653i
29. Hall EJ, Brenner DJ. The dose-rate effect revisited: radiobiological considerations of importance in radiotherapy. *Int J Radiat Oncol Biol Phys* **1991**; 21: 1403-14. https://doi.org/10.1016/0360-3016(91)90314-T
30. Steel GG, Down JD, Peacock JH, Stephens TC. Dose-rate effects and the repair of radiation damage. *Radiot Oncol* **1986**; 5: 321-31. https://doi.org/10.1016/s0167-8140(86)80181-5
31. Mitchell J, Bedford J, Bailey S. Dose-rate effects on the cell cycle and survival of S3 HeLa and V79 cells. *Radiat Res* **1979**; 79: 520-36. https://doi.org/10.2307/3575178
32. Darfarin G, Salehi R, Alizadeh E, Nasiri Motlagh B, Akbarzadeh A, Farajollahi A. The effect of SiO2/Au core–shell nanoparticles on breast cancer cell's radiotherapy. *Artif Cell Nanomed Biotechnol* **2018**; 46: 836-46. https://doi.org/10.1080/21691401.2018.1470526
33. Su X-Y, Liu P-D, Wu H, Gu N. Enhancement of radiosensitization by metal-based nanoparticles in cancer radiation therapy. *Cancer Biol Med* **2014**; 11: 86. https://doi.org/10.7497/j.issn.2095-3941.2014.02.003

34. Cai Z, Chattopadhyay N, Yang K, Kwon YL, Yook S, Pignol J-P, et al. 111In-labeled trastuzumab-modified gold nanoparticles are cytotoxic in vitro to HER2-positive breast cancer cells and arrest tumor growth in vivo in athymic mice after intratumoral injection. *Nucl Med Biol* **2016**; 43: 818-26. https://doi.org/10.1016/j.nucmedbio.2016.08.009
35. Maroufi NF, Vahedian V, Mazrakhondi SAM, Kooti W, Khiavy HA, Bazzaz R, et al. Sensitization of MDA-MBA231 breast cancer cell to docetaxel by myricetin loaded into biocompatible lipid nanoparticles via sub-G1 cell cycle arrest mechanism. *Naunyn-Schmiedeberg's Arch Pharmacol* **2020**; 393: 1-11. https://doi.org/10.1007/s00210-019-01692-5
36. Sabzichi M, Ramezani M, Mohammadian J, Ghorbani M, Mardomi A, Najafipour F, et al. The synergistic impact of quinacrine on cell cycle and anti-invasiveness behaviors of doxorubicin in MDA-MB-231 breast cancer cells. *Process Biochem* **2019**; 81: 175-81. https://doi.org/10.29252/mlj.14.4.38
37. Patra HK, Banerjee S, Chaudhuri U, Lahiri P, Dasgupta AK. Cell selective response to gold nanoparticles. *Nanomed: Nanotechnol Biol Med* **2007**; 3: 111-9. https://doi.org/10.1016/j.nano.2007.03.005
38. Matsuya Y, McMahon SJ, Tsutsumi K, Sasaki K, Okuyama G, Yoshii Y, Mori R, Oikawa J, Prise KM, Date H. Investigation of dose-rate effects and cell-cycle distribution under protracted exposure to ionizing radiation for various dose-rates. *Sci Rep* **2018**; 29; 8(1):1-4. https://doi.org/10.1038/s41598-018-26556-5
39. Hainfeld JF, Dilmanian FA, Zhong Z, Slatkin DN, Kalef-Ezra JA, Smilowitz HM. Gold nanoparticles enhance the radiation therapy of a murine squamous cell carcinoma. *Phys Med Biol* **2010**; 55: 3045. https://doi.org/10.1088/0031-9155/55/11/004
40. Rahman WN, Bishara N, Ackerly T, He CF, Jackson P, Wong C, et al. Enhancement of radiation effects by gold nanoparticles for superficial radiation therapy. *Nanomed: Nanotech Biol Med* **2009**; 5: 136-42. https://doi.org/10.1016/j.nano.2009.01.014
41. Butterworth K, Coulter J, Jain S, Forker J, McMahon S, Schettino G, et al. Evaluation of cytotoxicity and radiation enhancement using 1.9 nm gold particles: potential application for cancer therapy. *Nanotechnology* **2010**; 21: 295101. https://doi.org/10.1088/0957-4484/21/29/295101
42. Abdollahi BB, Malekzadeh R, Azar FP, Salehnia F, Naseri AR, Ghorbani M, et al. Main approaches to enhance radiosensitization in cancer cells by nanoparticles: A systematic review. *Adv Pharm Bull* **2021**; 11: 212. https://doi.org/10.34172/apb.2021.025
43. Kong T, Zeng J, Wang X, Yang X, Yang J, McQuarrie S, et al. Enhancement of radiation cytotoxicity in breast-cancer cells by localized attachment of gold nanoparticles. *Small* **2008**; 4: 1537-43. https://doi.org/10.1002/smll.200700794
44. Abhari F, Charmi J, Rezaeejam H, Karimimoghaddam Z, Nosrati H, Danafar H, et al. Folic acid modified bismuth sulfide and gold heterodimers for enhancing radiosensitization of mice tumors to X-ray radiation. *ACS Sustain Chem Eng* **2020**; 8: 5260-9. https://doi.org/10.1021/acssuschemeng.0c00182
45. Chattopadhyay N, Cai Z, Pignol J-P, Keller B, Lechtman E, Bendayan R, et al. Design and characterization of HER-2-targeted gold nanoparticles for enhanced X-radiation treatment of locally advanced breast cancer. *Mol Pharm* **2010**; 7: 2194-206. https://doi.org/10.1021/mp100207t